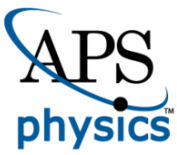

Search for microscopic and macroscopic biaxiality in the cybotactic nematic phase of new oxadiazole bent-core mesogens

Young-Ki Kim, Greta Cukrov, Francesco Vita, Eric Scharrer, Edward T. Samulski, Oriano Francescangeli, and Oleg D. Lavrentovich

Phys. Rev. E **93**, 062701 — Published 1 June 2016

DOI: 10.1103/PhysRevE.93.062701

Search for Microscopic and Macroscopic Biaxiality in the Cybotactic Nematic Phase of New Oxadiazole Bent-Core Mesogens

Young-Ki Kim,[1, *] Greta Cukrov,[1] Francesco Vita,[2] Eric Scharrer,[3] Edward T. Samulski,[4] Oriano Francescangeli,[2, †] and Oleg D. Lavrentovich[1, †]

[1] *Liquid Crystal Institute and Chemical Physics Interdisciplinary Program, Kent State University, Kent, OH 44242, USA*

[2]*Dipartimento di Scienze e Ingegneria della Materia, dell'Ambiente ed Urbanistica and CNISM, Università Politecnica delle Marche, Via Brecce Bianche, 60131, Ancona, Italy*

[3]*Department of Chemistry, University of Puget Sound, 1500 N. Warner, Tacoma, WA 98416, USA*

[4] *Department of Chemistry, University of North Carolina, Chapel Hill, NC 27599-3290, USA*

[*] Current address: Department of Chemical & Biological Engineering, University of Wisconsin-Madison, Madison, WI 53706, USA

[†] Corresponding Authors: o.francescangeli@univpm.it; olavrent@kent.edu

Abstract.

The possibility of biaxial orientational order in nematic liquid crystals is a subject of intense current interest. We explore the tendencies toward local and global biaxial ordering in the newly synthesized trimethylated oxadiazole-based bent-core mesogens with a pronounced asymmetric (bow-type) shape of molecules. The combination of X-ray diffraction and optical studies suggest that the biaxial order is expressed differently at the short- and long-range scales. Locally, at the scale of a few molecules, X-ray diffraction data demonstrate biaxial packing. However, above the mesoscopic scale, the global orientational order in all three compounds is uniaxial, as evidenced by uniform homeotropic alignment of the nematic phase as optically tested over the entire temperature range, and by the observations of topological defects induced by individual and aggregated colloidal spheres in the nematic bulk.

I. INTORODUCTION

Bent-core nematics (BCNs) [1] are currently being explored by several groups worldwide because of their unusual properties and the potential for finding new regimes in which they can operate better than conventional liquid crystals (LCs) formed by rod like molecules. Due to their bow shape that naturally specifies a secondary direction for orientational ordering (orthogonal to the primary or uniaxial director **n**), their potential to exhibit the elusive biaxial nematic (N_b) phase is undoubtedly the most fascinating feature [2]. So far, however, an impressive range of studies has drawn disparate conclusions on the issue of biaxiality, and the assessment of the N_b phase in BCNs is a topic still controversial and widely debated [3-16]. Nevertheless, biaxiality is closely related to the nature of short-range intermolecular order in BCNs, an issue that has equally generated both great interest and lively debate within the LC community in recent years. In this regard, a general consensus has emerged that the unconventional behavior of BCNs is due to the cybotactic nature of their nematic (N) phase [17-30].

The cybotactic model of the N phase assumes the existence of short-range smectic (Sm)-like ordering in the form of nanometer-sized clusters (cybotactic groups) exhibiting a layered supramolecular structure (typically skewed, i.e. SmC-like) with intrinsic biaxial orientational order. Recent X-ray diffraction (XRD) experiments performed by some of the present authors have provided the first direct evidence of *local* (i.e. on the length scale of the cybotactic cluster size) biaxial order in the N phase of a pair of trimethylated BCNs based on the 1,3,4-oxadiazole bisphenol (ODBP) mesogenic core (compounds **2**, **3** in Fig. 1) [31, 32]. This was inferred from the splitting of the wide-angle (WA) diffuse crescents in the XRD pattern of the N phase oriented in a magnetic field **B** orthogonal to the X-ray beam. Such splitting corresponds to two different transverse intermolecular distances in the plane orthogonal to the magnetically aligned primary

director **n**||**B**. The effect is strongly correlated to the peculiar lateral substitution pattern of the investigated mesogens: in fact, it is not observed either in the parent unmethylated compound nor in monomethylated derivatives such as compound **1** in Fig. 1; on the other hand, it persists if the inner methyl group is replaced by a halogen [33] and also shows up in trimethylated compounds based on an oxazole bisphenol moiety [34]. Interestingly, all BCNs showing the WA splitting can be supercooled to room temperature in a metastable, highly viscous N state; the splitting increases with decreasing temperature. The importance of such a finding is twofold. First, it demonstrates that XRD is not *blind* to biaxiality in BCNs, even when the two transverse intermolecular distances differ by only $\sim 1\,\text{Å}$. Secondly, the fact that local biaxial order was hitherto experimentally accessed only in a restricted family of laterally substituted derivatives implies the existence of a structure-enhanced orientational correlation in the transverse molecular packing, which makes these materials very promising candidates in the search for long-range macroscopic biaxiality. However, those previous experiments were not primarily designed to probe the transverse molecular ordering, thus preventing further speculations on the spatial scale of the extent of such biaxial order.

In this paper, we have applied XRD with a setup optimized to probe the transverse molecular ordering, by subjecting the compounds **1-3** to a magnetic field, $\mathbf{B}$, parallel to the direction of the X-ray incident beam and collecting the scattered intensity in the plane normal to such direction. Additionally, in order to elucidate the true nature of the N phase, uniaxial or biaxial, we have performed an extended optical characterization of surface alignment and topological defects of the above BCNs. The XRD data confirm the existence of microscopic local biaxial order but do not provide any detectable evidence of macroscopic biaxiality. On the

other hand, the optical studies show that on the macroscopic scale the BCNs behave as uniaxial nematics (N_u).

II. RESULTS AND DISCUSSION

A. Materials and techniques

Figure 1 shows the chemical structures and phase diagrams of the investigated ODBP BCNs, **(1)** monomethylated OC4-Ph(mono2MeODBP) and **(2)** trimethylated OC4-2MePh(mono2MeODBP) and **(3)** OC4-2MePh(mono3MeODBP). Their synthesis, phase behavior, and structural characterization have been previously described [35]: while all of them exhibit an enantiotropic cybotactic N phase, trimethylated compounds **2**, **3** show much lower N onset temperatures and a propensity for supercooling the cybotactic order down to room-temperature in a metastable, highly viscous state. Compounds **2**, **3** are those for which direct XRD evidence of local biaxial order was first reported in 2014 [31]. Compound **1** is a BCN of the same family that, unlike the previous two, does not exhibit similar evidence and is reported here only for the sake of comparison.

The phase diagrams shown in Fig. 1 were established by polarizing optical microscopy (POM) upon both heating and cooling. The diagrams are consistent, within $1-5\ ^{o}C$, with the previous studies [31, 35] except for the limit of supercooling (nematic - crystal (Cr) transition upon cooling) that varies from cell to cell.

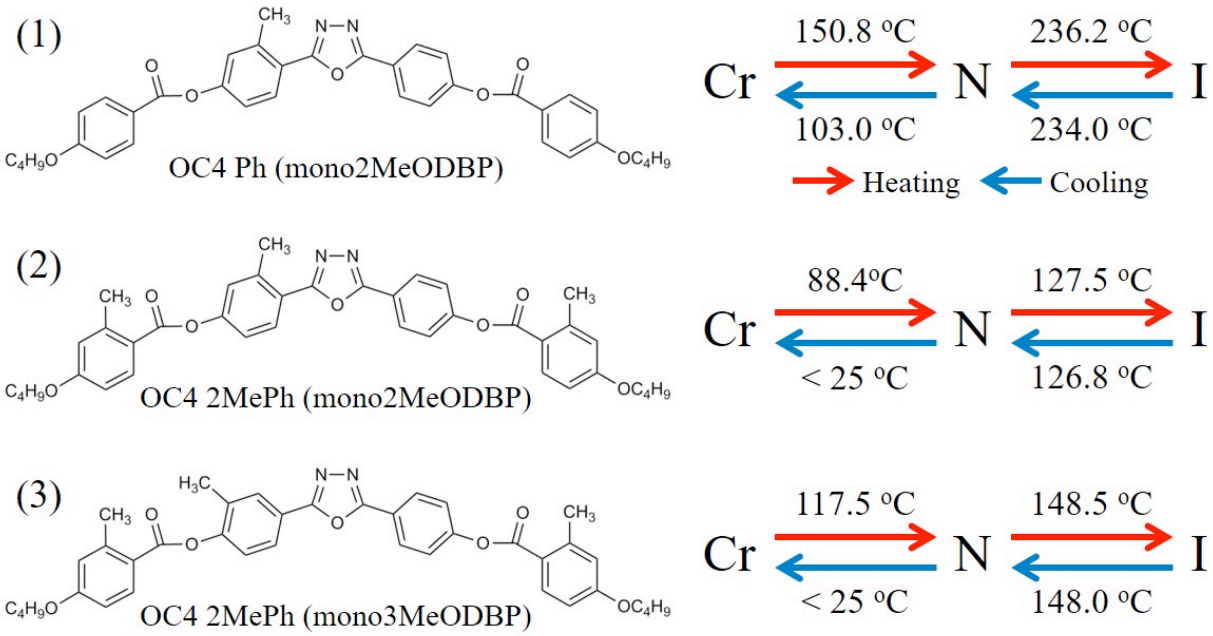

FIG. 1. Chemical structures and phase diagrams of the new ODBP bent-core nematic liquid crystals, (**1**) OC4-Ph(mono2MeODBP), (**2**) OC4-2MePh(mono2MeODBP), and (**3**) OC4-2Meph(mono3MeODBP); Cr, N, and I represent crystal, nematic, and isotropic phases, respectively.

XRD measurements were performed at the BM26B DUBBLE beamline of the European Synchrotron Radiation Facility (ESRF) in Grenoble, France. BCNs **1-3** were placed in capillaries (1.5 mm diameter) and mounted in a temperature-controlled hot stage (precision better than 0.1 °C). Two magnets allowed a static magnetic field **B** ($B = 0.83$ T, measured in air) to be applied across the sample, perpendicularly to the capillary and parallel to the incident X-ray beam. The diffraction patterns were collected using a two-dimensional CCD camera. The beam size was $300 \times 300\ \mu m^2$, the wavelength $\lambda = 1.033$ Å and the sample-to-detector distances was 136 mm.

In the experiments for optical characterization we explored two types of nematic samples, sandwiched cells with two glass substrates with (a) a homeotropic alignment and (b) a planar alignment containing colloidal inclusions; the terms "homeotropic" and "planar" refer to the normal and tangential alignment of the main director **n** at the bounding plates. Since oxadiazole LCs were reported to experience a strong thermal degradation in an oxygen environment, all experiments have been carried out with fresh cells within 5 hours or less [12, 16]. In order to avoid any possible memory effect [12], all experiments were performed above the Cr-N phase transition temperature. The temperature was controlled by a hot stage LTS420 and a controller T95-HS (both Linkam Instruments) with an accuracy of $0.01\ ^{o}\mathrm{C}$. We adopted the slow rate of temperature change, $\pm 0.5\ ^{o}\mathrm{C}/\min$, to minimize the material flow by thermal expansion that can mimic the features of $\mathrm{N_b}$ [15, 36, 37].

B. X-ray diffraction

Figure 2(a) shows the XRD pattern of BCN **1** in the N phase (at temperature $T = 155\ ^{o}\mathrm{C}$) as a representative example of the scattering that is generally observed in bent-core mesogens. The broad diffuse ring in the WA scattering region is associated with the transverse molecular ordering, i.e. the molecular ordering in the plane normal to the molecular director **n** (**n**||**B**). By contrast, Figures 2(c) and 2(e) show the XRD pattern of BCN **2** in the fluid ($T = 100\ ^{o}\mathrm{C}$) and in the supercooled ($T = 30\ ^{o}\mathrm{C}$) N phase, respectively. A very similar pattern (not reported here) was found for BCN **3**. The different behavior of BCNs **2**, **3** compared to conventional BCN **1** becomes apparent in the intensity profile obtained from the radial scan of the pattern. Figures 2(b), 2(d), and 2(f) show the intensity (I) vs modulus of the scattering vector (q), I vs q,

curve obtained after azimuthal integration of the XRD patterns in Figures 2(a), 2(c), and 2(e), respectively, over a π range. While in the WA region BCN **1** exhibits a single symmetric diffuse peak centered at $q = 14.3\,\mathrm{nm}^{-1}$ (corresponding to a *d*-spacing $d = 2\pi / q = 4.4\,\text{Å}$), typical of conventional nematics of rod-like molecules, BCN **2** shows an asymmetric broad diffuse feature consisting of the superposition of two distinct wide diffraction peaks, p_1 and p_2, centered about two significantly different values of q. The quantitative analysis performed by fitting the profiles with Voigt lineshapes provides the values $q_1 = 12.4\,\mathrm{nm}^{-1}$ and $q_2 = 16.2\,\mathrm{nm}^{-1}$, corresponding to the intermolecular distances $d_1 = 5.0\,\text{Å}$ and $d_2 = 3.9\,\text{Å}$ at $T = 100\,^{\circ}\mathrm{C}$ as well as $q_1 = 12.2\,\mathrm{nm}^{-1}$ and $q_2 = 16.6\,\mathrm{nm}^{-1}$, corresponding to the intermolecular distances $d_1 = 5.1\,\text{Å}$ and $d_2 = 3.8\,\text{Å}$, at $T = 30\,^{\circ}\mathrm{C}$. Similar results were found for BCN **3**, confirming the peculiar behavior of both BCNs **2**, **3**.

The existence of two distinct intermolecular distances represents undisputable proof of local biaxial packing in the N phase of BCNs **2**, **3**. In fact, d_2 corresponds to the typical face-to-face distance between stacked π-systems whereas d_1 is closer to the width of a planar aromatic ring, in accordance with the molecular packing depicted in Figure 3. Additional information on the short-range (anisotropic) positional order of the mesogens is provided by the two correlations lengths, ξ_1 and ξ_2, along the minor transverse directors $\mathbf{l}, \mathbf{m}$ [Fig. 3], respectively. Following Ref. [38], these were calculated as $\xi_i = 9.92 / \Delta q_i \ (i = 1, 2)$, where Δq_i is the full width at half maximum (FWHM) of the p_i diffraction peak. For BCN **2** this gave the values $\xi_1 = 10.2\,\text{Å} \approx 2d_1$ and $\xi_2 = 17.3\,\text{Å} \approx 4d_2$ at $T = 100\,^{\circ}\mathrm{C}$ and $\xi_1 = 11.5\,\text{Å} \approx 2d_1$ and $\xi_2 = 19.1\,\text{Å} \approx 5d_2$ at $T = 30\,^{\circ}\mathrm{C}$ (similar values were obtained for BCN **3**). For the sake of

comparison, the same calculations for BCN **1** at $T = 155$ °C provided the value $\xi = 11.5$ Å $\approx 3d$. Apparently, these results show that in BCNs **2**, **3** the close packing constraints favor the face-to-face stacking of aromatic cores more strongly than their in-plane arrangement.

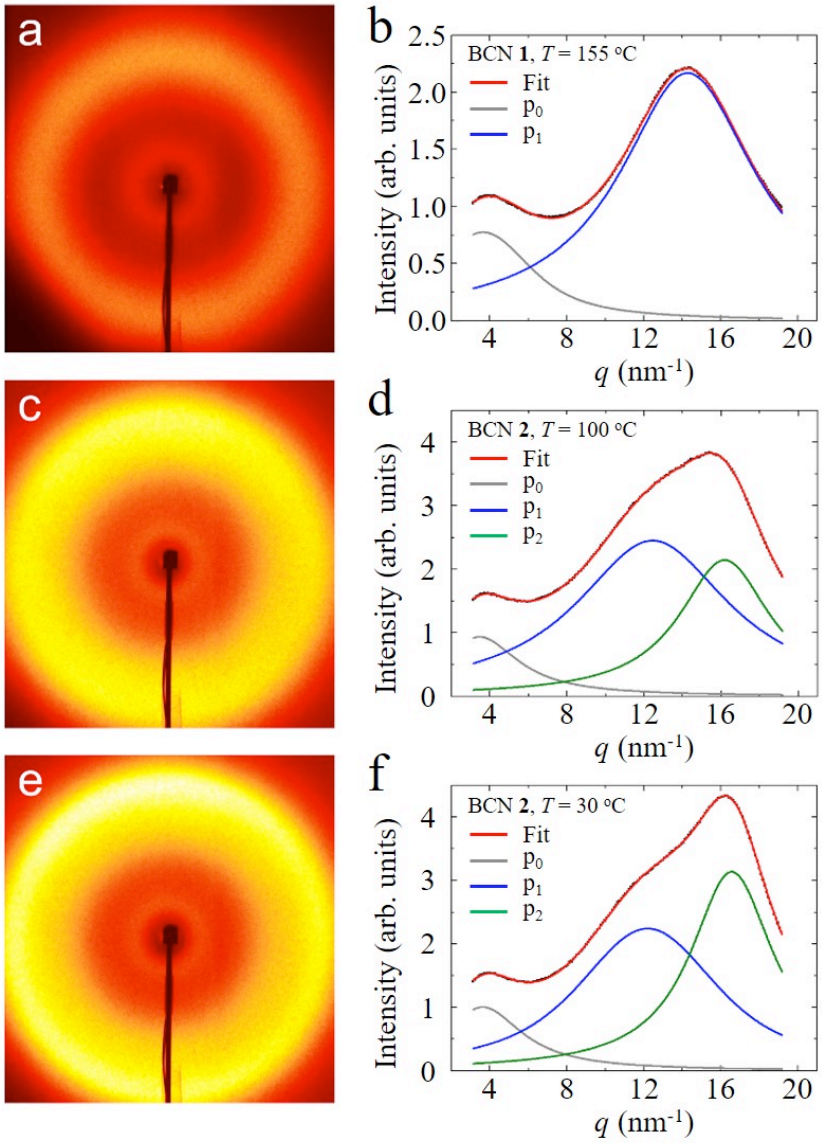

FIG. 2. (a,c,e) XRD patterns measured with **B** parallel to the X-ray beam and fits of the corresponding radial intensity profiles (averaged over a π azimuthal angle) with (b) two or (d,f) three Voigt lineshapes: (a,b) BCN **1** at 155 °C; (c,d) BCN **2** at 100 °C; (e,f) BCN **2** at 30 °C.

With this initial assessment of local biaxial ordering, our interest next turned to the spatial extent of such order. i.e. whether it is restricted to the short-range scale or, instead, persists over macroscopic length scales (long-range order), in which case we could speak of true N_b phase. It is important to observe that *short-range* and *long-range* here refer to the molecular length scale and, unless external aligning fields (mechanical, electric, magnetic) are applied to the sample, the orientational order of a fluid LC phase spontaneously extends over domains that typically do not exceed the micron-size. Accordingly, biaxiality is considered macroscopic if the biaxial order extends to the length scale of the LC micro-domains. However, only when such micro-domains are coherently oriented by an external field, would one get a monodomain biaxial sample.

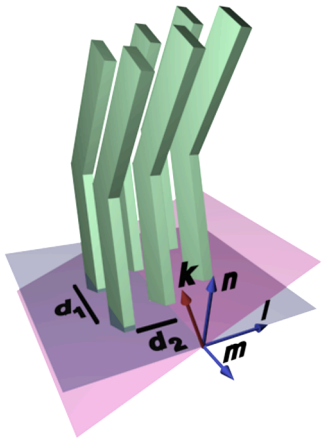

FIG. 3. Schematic drawing of the molecular ordering within a cybotactic cluster: **k** indicates the normal to the smectic plane (purple), **n**, **m** and **l** are the three orthogonal molecular directors; d_1 and d_2 are the intermolecular distances in the plane normal to **n** (grey).

The situation becomes subtler for cybotactic nematics where the aggregation of molecules into clusters introduces an additional length scale, i.e. the average dimension of the cybotactic clusters, intermediate between the molecular and the micro-domain size. In this frame, biaxial order is considered *local* if limited to the length scale of the cybotactic cluster size (a few nanometers), and *macroscopic* if it extends to the micro-domain size. With a biaxial monodomain sample having the transverse molecular directors ($\mathbf{l}$, $\mathbf{m}$) uniformly aligned over the probed sample volume [Figure 4(a)], the XRD peaks p_1 and p_2 would appear azimuthally focused, with the respective maxima centered along mutually orthogonal directions, as shown in Figure 4(b). In the absence of a transverse aligning field, as it is in our experiment, a macroscopically N_b phase would consist of biaxial micron-sized domains (each one consisting of uniformly aligned cybotactic clusters) with minor molecular directors ($\mathbf{l}$, $\mathbf{m}$) randomly distributed about the primary director $\mathbf{n}$ [Figure 4(c)]. In this case, p_1 and p_2 peaks would spread out into azimuthally isotropic rings [Figure 4(d)] and this pattern would be indistinguishable from that of a *composite* N_u [18], i.e. one composed of biaxial clusters with random distribution of the transverse axes about $\mathbf{n}$. However, any small preferential orientation of the micro-domains in the transverse plane (spontaneous or occasionally induced) would reflect in azimuthal modulations (with period π) of the ring intensity of p_1 and p_2 that are shifted by $\pi/2$ as shown in Figure 4(b), with the maxima of p_1 and p_2 located along two mutually orthogonal directions. Accordingly, a small but detectable azimuthal intensity modulation with the above features could be used to demonstrate the macroscopic biaxial nature of the N.

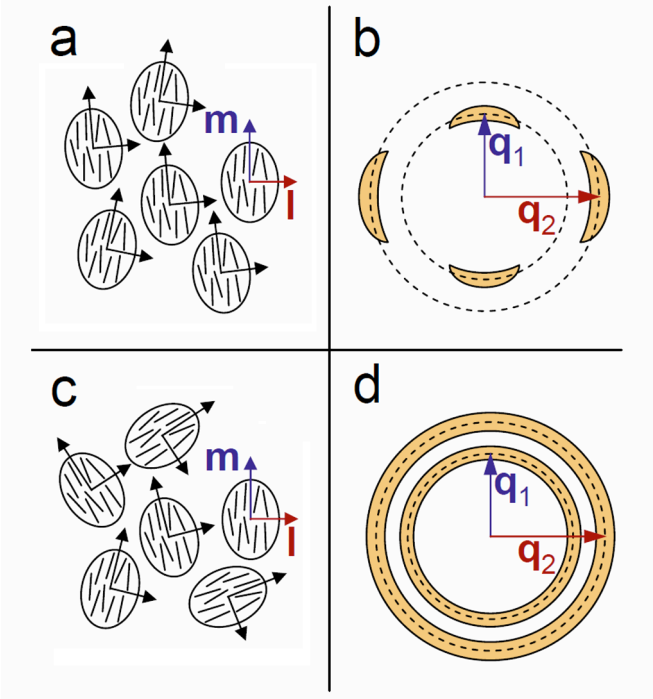

FIG. 4. Orientation of the transverse molecular directors **m** , **l** in N_b with **n** perpendicular to the drawing: transverse directors aligned by (a) an external field or (c) randomly distributed in the plane orthogonal to **n** . The ellipses represent micron-sized domains (each one consisting of uniformly aligned nanometer-sized cybotactic clusters) where the orientation of the molecular director is spontaneously uniform. (b) and (d) show the corresponding WA diffraction patterns. The latter would be indistinguishable from that of a composite N_u comprised of randomly oriented nano-sized biaxial clusters.

To check this possibility, the azimuthal intensity profiles of p_1 and p_2 were measured for BCN **2** (at 100 °C and 30 °C) and compared with the WA azimuthal intensity profile of BCN **1** (at 155 °C). Figure 5 shows the azimuthal profiles obtained by integrating the XRD patterns over radial q-intervals of $0.2\,\mathrm{nm}^{-1}$ centered on the peak maxima. The intensities in Figure 5 are

not azimuthally constant, even in the case of BCN **1** (where no modulation is expected), because of spurious experimental effects (sample inhomogeneities, misalignments, errors introduced by the background subtraction, etc.). Nevertheless, the phase-shifted π-periodic modulations expected for N_b [Fig. 4(b)] are clearly not evident in these profiles. On this basis, we can conclude that although the XRD data do not completely rule out macroscopic biaxiality (the case in which the azimuthal modulations are inexistent or too small to be detected over the *noisy* background), they actually do not provide any clear proof of macroscopic biaxial order. The following optical characterization was performed to gain complementary information aimed at establishing whether the local biaxiality revealed by XRD can extend to macroscopic scales thus producing a thermodynamically stable N_b.

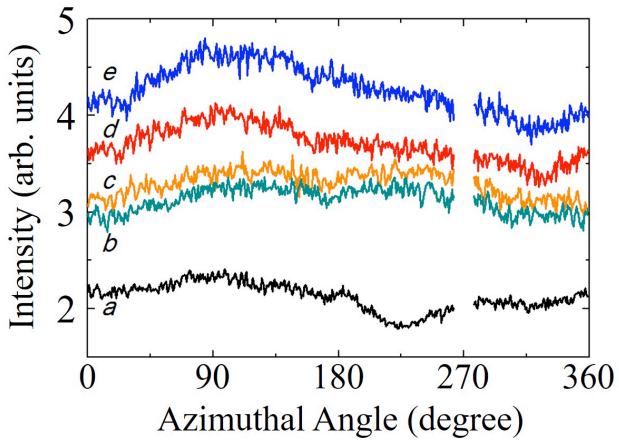

FIG. 5. Azimuthal intensity profiles of the WA peaks shown in the fits of Figure 2: peak p_1 of BCN **1** at 155 °C (curve a); peak p_1 (curve c) and p_2 (curve d) of BCN **2** at 100 °C; peak p_1 (curve b) and p_2 (curve e) of BCN **2** at 30 °C. The gap at 270 degree is due to the shadow of the beamstop.

C. Optical characterization of homeotropic cells

A straightforward approach to distinguish between N_u and N_b is to probe a cell with homeotropic alignment of the main director **n**. If the nematic is uniaxial, then such a homeotropic cell viewed between two crossed linear polarizers appears dark, since only one mode (ordinary) of propagation is allowed and the optical retardation is zero. If the nematic is biaxial, then there is a non-zero optical retardation $\Gamma = \Delta n_{\text{eff}}\, h$ caused by in-plane birefringence Δn_{eff} associated with the secondary directors **l** and **m**; h is the cell thickness. The N_b cell, viewed between two crossed polarizers, would be partially transparent, with the intensity of light transmitted through the cell and two crossed polarizers being proportional to $\sin^2\left(\pi \Delta n_{\text{eff}}\, h / \lambda_0\right)$, where λ_0 is the wavelength of light in vacuum, see, for example Ref. [39]. Thus the appearance of macroscopic biaxiality in a homeotropic cell can be detected by measuring the optical phase retardance $\Gamma = \Delta n_{\text{eff}}\, h$ or the intensity of light passing through the cell and the two crossed polarizers. The phase retardance can be measured in the so-called LC PolScope mode of polarizing microscopy observations [40, 41], with accuracy better than $0.05\,\text{nm}$.

Homeotropic alignment of nematics formed by molecules of nontrivial shape, such as bent-core BCNs **1**, **2**, and **3**, is not a trivial task. For example, polyimides SE1211, SE7511, and SE5661 (Nissan Chemical Industries) that are widely used to align **n** homeotropically for many liquid crystals, produce only Schlieren textures for BCNs **1-3**, with numerous linear, point, and wall defects, Figs. 6(a)-6(c). To achieve homeotropic alignment of compounds **1-3**, we used an approach based on addition of a UV-curable reactive mesogen (RM) to the polyimide aligning layer [42]. This approach has been already successfully demonstrated for homeotropic alignment of many other nematics with complex molecular shapes, such as tetrapodes [43-45],

H-shaped [46], bent-core mesogens ODBP-Ph-C_7 and ODBP-Ph-C_{12} [4, 12], A131 [9], and CB7CB [47, 48]. The reactive mesogen RM-257 (Merck) was added to the polyimide SE5661 in 1:50 weight proportion. To this mixture, a small amount (0.1 in weight proportion) of photo-initiator Irgacure 651 (Ciba Chemicals) was added in order to enhance the photo-reactivity. RM-SE5661 mixture was spin-coated on glass plates and baked at 170 °C for 60 min. Subsequently, RM-SE5661 coated substrates were exposed to UV irradiation using 6 Watts UV lamp (UVL-56, UVP) for 90 minutes in order to polymerize the RM. The cells assembled with RM-SE5661 plates showed homeotropic alignment of all studied BCN materials. The cell gap was set by glass spacers mixed with UV glue (Norland Optical Adhesive 65, Norland Products, Inc.) that was also used to seal the cell edges.

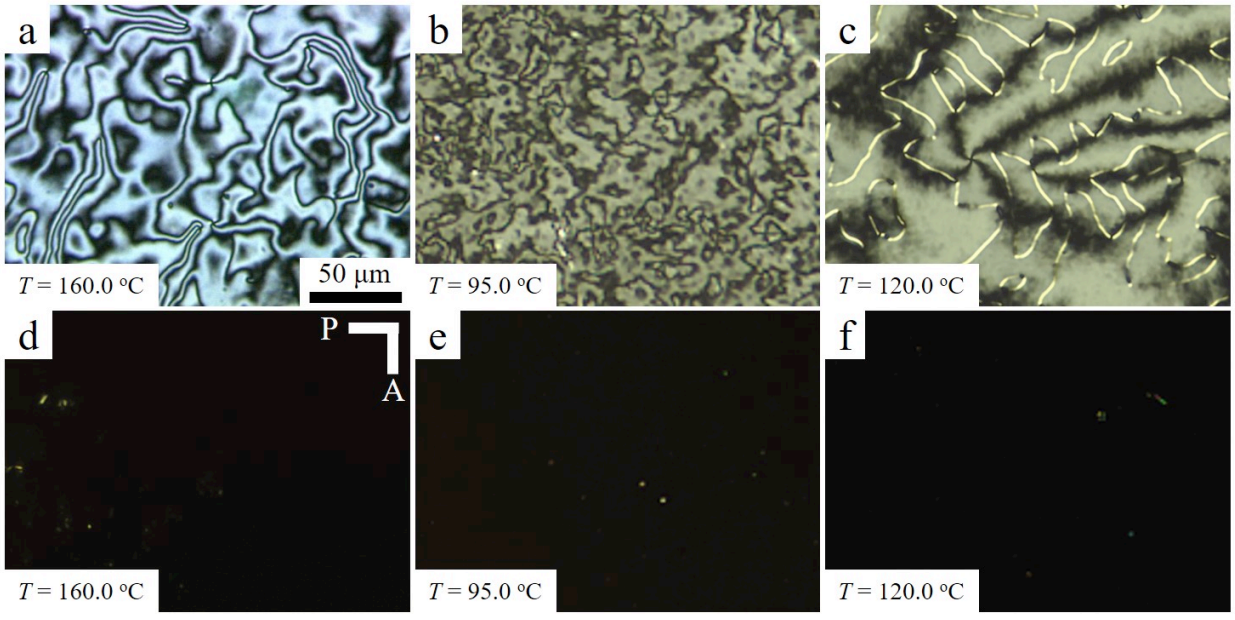

FIG. 6. POM textures of the BCNs **1-3** in (a-c) SE5661 and (d-f) RM-SE5661 cells of $h = 1.3\,\mu\text{m}$. Left column is with BCN **1** at $T = 160.0\,^{\circ}\text{C}$, central column is with BCN **2** at

$T = 95.0\ ^{o}\mathrm{C}$, and right column is with BCN **3** at $T = 120.0\ ^{o}\mathrm{C}$. P and A indicate the polarization of polarizer and analyzer, respectively.

Figures 6(d)-6(f) show POM textures of BCNs **1**,**2**,**3** cells exhibiting homeotropic alignment in the entire N phase, recorded at selected representative temperatures. Thin cells ($h = 1.3\ \mu\mathrm{m}$) remain dark when viewed between crossed polarizers in the entire range of the nematic phase, indicating a uniaxial orientational order. Thicker cells, $h > 3\ \mu\mathrm{m}$, however, exhibit the homeotropic dark textures only in a certain temperature range, $T^* < T < T_{\mathrm{NI}}$, between the melting point T_{NI} and a critical temperature T^* below which the sample becomes birefringent and shows defects. The value of T^* increases as d increases. This thickness dependent T^* suggests that the transition from dark to birefringent texture at T^* is associated with the surface anchoring transition, i.e., a tilt of director **n** in $\mathrm{N_u}$, rather than the phase transition from $\mathrm{N_u}$ to $\mathrm{N_b}$. Similar surface anchoring transitions in $\mathrm{N_u}$ materials that mimic $\mathrm{N_b}$ behavior have been observed in other materials [16, 45, 46]. The thickness dependence of the anchoring transition temperature T^* can be attributed to the effect of electric double layers formed by ionic impurities in the material, as explained in Ref. [16]. Since the dielectric anisotropy of studied BCNs is negative, the electric field of double electric layers tends to align the director perpendicularly to itself, i.e., tangentially. This tendency is stronger in thick cells, in which the double layers are fully developed. As discussed in details in Ref. [16], in thin cells, the surface density of charges is lower and the tendency for the tangential anchoring is weakened, which explains why the thin cells show stable homeotropic alignment in the entire range of the nematic phase, including the supercooled regions.

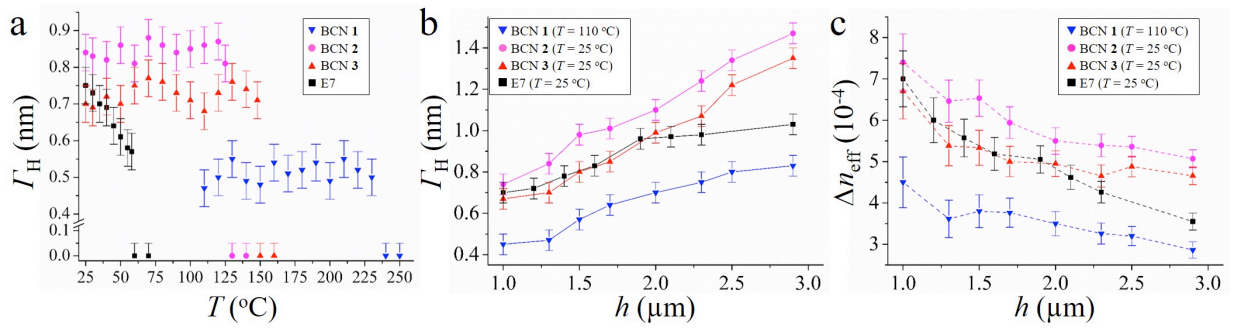

FIG. 7. Optical properties of the homeotropic RM-SE5661 cells filled with BCNs **1**, **2**, and **3**, and the standard N_u mixture E7. (a) Optical retardance Γ_H vs. temperature T in cells of thickness $h = 1.3\,\mu m$; (b) Γ_H vs cell thickness h for the temperatures presented in the figure; (c) effective in-plane birefringence $\Delta n_{eff} = \Gamma_H / h$ as a function of h at selected temperatures. Data were recorded upon cooling within the N phase, including the supercooled N region.

To quantify the upper limit of in-plane birefringence Δn_{eff} in the homeotropic cells, the optical retardance $\Gamma_H = \Delta n_{eff} h$ was measured using LC PolScope (Abrio Imaging System) [41, 49, 50]. The measurements were performed for all three BCN materials and also for the standard N_u LC mixture E7 (Merck). Figure 7(a) shows the temperature dependence of Γ_H measured in the homeotropic RM-SE5661 cells of thickness $h = 1.3\,\mu m$. In the entire temperature range of the N phase for all four materials, the measured Γ_H is vanishingly small, well below $1\,nm$. As the temperature decreases, Γ_H shows a small increase for E7 and practically no change for BCNs **1**-**3**; the latter result is not consistent with the biaxial behavior, as in the N_b phase, Γ_H should increase as the temperature is reduced, because of the in-plane birefringence increase.

The data suggest that the small Γ_H measured in BCNs **1-3**, which is of the same order of magnitude as Γ_H in a classic N_u E7, is caused by factors other than the macroscopic biaxial order. Among these factors might be director distortions at small imperfections such as dust particles, irregularities of the substrates, and director fluctuations.

The conclusion about a non-biaxial nature of the residual retardance Γ_H is confirmed in the experiments in which Γ_H is measured as a function of the cell thickness h, Fig. 7(b). In N_b, biaxiality-induced birefringence $\Delta n_{eff} = \Gamma_H / h$ should be a constant independent of h, as it characterizes the material property. However, the data, Fig. 7(c), show that the value Γ_H / h for all four materials, including E7, decreases as the cell thickness increases, remaining very low, on the order of 10^{-4}. Such thickness dependence can be expected when the light leakage through the cell is caused mostly by surface imperfections, since their effect on the director is stronger in thinner cells.

We conclude that the optical features of homeotropic textures of BCNs **1-3** are consistent with the uniaxial orientational order in the entire nematic range of these materials; their optical properties are practically indistinguishable from those of the standard N_u E7. In the next section, we perform an independent test of the macroscopic orientational order of BCNs **1-3** by exploring topological defects around colloidal spheres embedded into the planar cells.

D. Study of topological defects caused by colloids in planar cells

The N_u and N_b phases show very different sets of topological defects [39, 51, 52] because of the difference in the symmetry of their orientational order. One of the approaches to

discriminate between N_u and N_b is to observe the topological defects formed around colloidal spheres immersed in the uniform LC cell. If the surface of the sphere provides a tangential alignment, the director field at this surface must contain singularities of a total strength $\sum_i m_i$ equal to 2, according to the Poincaré theorem [39]. In the N_u case, the theorem is satisfied by two point defects, called boojums, of charge $m = 1$ each, located at the two poles of the spheres, Figure 8(a). In the N_b phase, however, these point defects cannot exist and the relationship $\sum_i m_i = 2$ can be satisfied either by a pair of singular lines (disclinations) of strength $m = 1$ each, emanating from the poles of the colloid, Figure 8(b), or by a single point defect-boojum of double strength $m = 2$ (not shown).

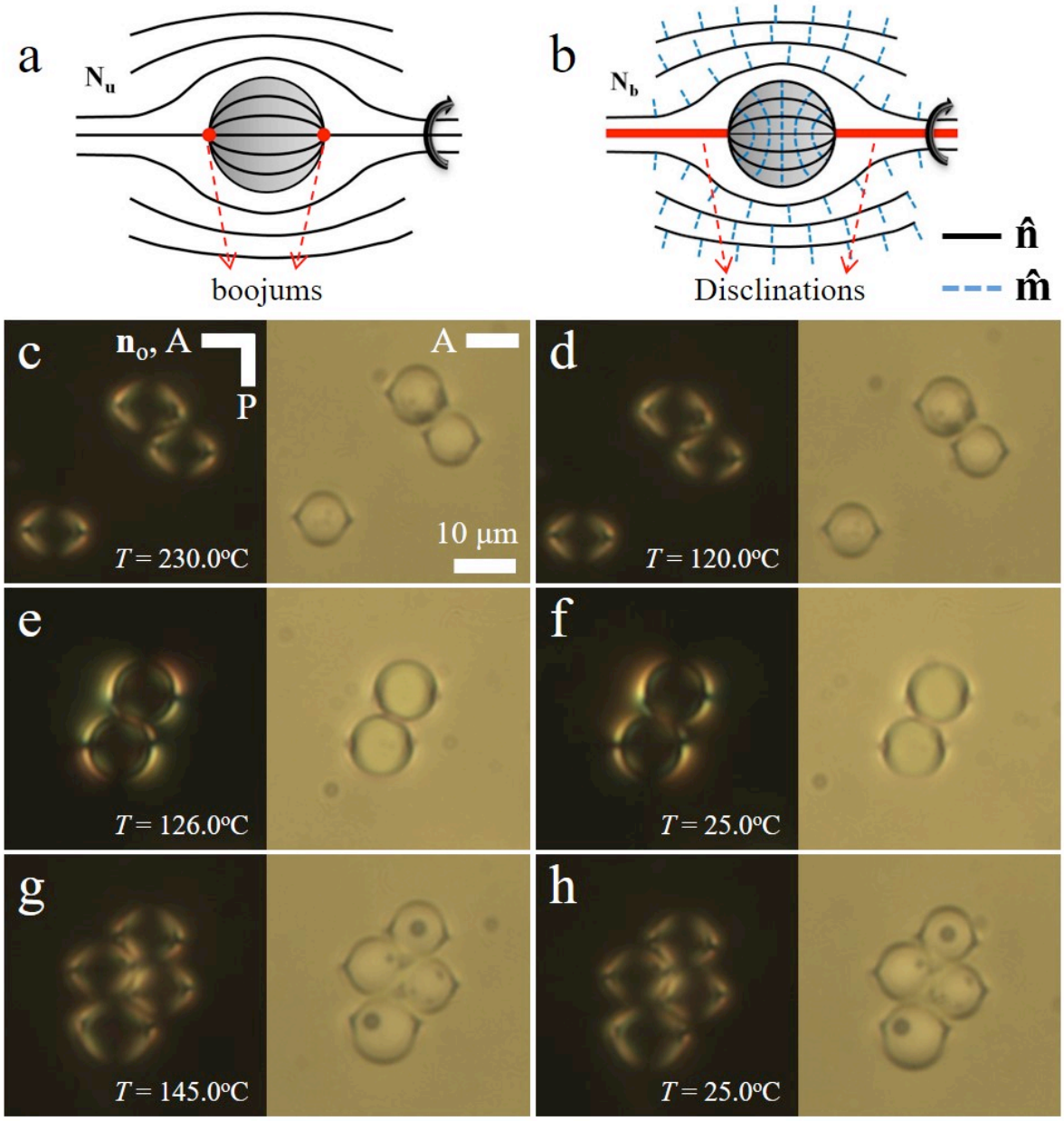

FIG. 8. (a) Scheme of the director configuration around a sphere with tangential alignment placed in a planar N_u cell; note two point defect-boojums at the poles; (b) a hypothetical configuration of the main and secondary director around a similar sphere placed in a N_b cell. Note two disclination lines in the secondary director emerging from the poles. (c-h) POM textures of isolated glass spheres and their clusters in the planar N cells ($h = 20\,\mu m$) at the

temperatures indicated on the figures; (c, d) BCN **1** ; (e, f) BCN **2** ; (g, h) BCN **3**. P, A, and $\mathbf{n}_0$ represent the polarization of polarizer and analyzer, and the overall director set by the rubbing direction.

To investigate the defect features in the studied BCNs, borosilicate glass spheres of diameter $D = 10\,\mu m$ were dispersed in the uniform cells with planar alignment, imposed by the rubbed layer of a polyimide PI2555 (HD Microsystems). The cells were of thickness $h = 20\,\mu m$. All colloids dispersed in the BCNs **1**-**3** nematic cells show two point defects, boojums, at their poles that are stable in the entire temperature range of the N phase, including the super-cooled regions, Figures 8(c)-8(h). These textures are the same as those observed for tangentially anchored sphere in normal N_u materials [53-56]. More precisely, an isolated sphere shows two symmetric point defect-boojums each of a strength $m = 1$ located at the poles; the axis that connects them is parallel to the overall director. The tangential alignment at the particles' surface is spontaneous in BCNs **1**-**3**. Note that tilted alignment would introduce an additional defect, a disclination loop at the equator, or make the two boojums asymmetric with respect to each other, as follows from the analysis of director fields defined at spherical surfaces [57]. The experimental textures, Figures 8(c)-8(h) are of a pure quadrupolar form, with symmetric boojums and no disclination loop, which confirms spontaneous tangential orientation.

Although the observed textures are fully consistent with the uniaxial long-range order of the material, they are incompatible with the topological defect structures required by a colloidal sphere placed in the biaxial N_b slab. The symmetry of the N_b phase prohibits existence of the boojums of strength $m = 1$ as isolated point defects for any type of anchoring for the main

director (tangential, tilted or homeotropic). As discussed above, these point defects should be associated with disclinations, caused by the secondary directors if the material were in the N_b phase, as sketched hypothetically in Fig. 8(b) for the case when the main director is aligned tangentially. We do not observe any disclination lines terminating at the boojums that might have been caused by the biaxial orientational order. In principle, one might argue that the disclinations do exist, but they are of a poor optical contrast and are not visible under the POM. However, their presence should manifest itself in how two or more neighboring spheres interact with each other. If the disclinations were present, one would observe pole-to-pole chaining of the spheres along their axes; such a chaining would minimize the length of disclinations and thus the elastic energy. Instead, we observe titled arrangement of the neighboring colloids, in which the centers of spheres are located along a line that forms a significant angle (40-60 degrees) with the overall director $\mathbf{n}_o$. The boojums at the poles of the neighboring spheres do not attract to other boojums. Such a tilted arrangement is characteristic of a quadrupolar interaction of tangentially anchored spheres in N_u [53-56]. The tilted arrangement of spheres remains stable in the entire temperature range of the N phase, Figs. 8(c)-8(h), confirming the conclusion about the uniaxial character of the N order.

III. CONCLUSIONS

We investigated the nano-structural, optical, surface, and topological properties of newly synthesized oxadiazole BCNs, referred to as BCNs **1**, **2**, and **3**, in order to verify the existence of macroscopic biaxial nematic (N_b) order. The XRD data confirm microscopic biaxiality on the local scale but do not provide any evidence of macroscopic biaxiality. Using a reactive mesogen

doped polyimide, all three materials could be aligned in a homeotropic fashion over the entire temperature range of the nematic phase implying a uniaxial nematic (N_u) phase. The negligibly small value of optical retardance Γ_H and the effective birefringence $\Delta n_{eff} = \Gamma_H / h$ measured in the homeotropic cell of BCNs **1-3** materials support the conclusion that the orientational order is uniaxial over the entire range of the nematic phase. Topological defects that are formed in the presence of colloidal spheres in the nematic bulk of BCNs **1-3** are of the same type observed in regular uniaxial nematics, i.e., surface point-defects boojums of strength 1 that are topologically prohibited in N_b. The colloidal spheres show a quadrupolar type of inter-sphere interactions and aggregate in a tilted fashion as they do in N_u.

We thus conclude that all three BCNs **1-3** do not exhibit macroscopic biaxiality in the nematic phase including the region of the supercooled nematic. Thus the local biaxial ordering of the molecules, clearly evidenced in the X-ray experiment, coexists with global uniaxial orientational order. Given the unequivocal local biaxiality in this unique class of BCNs, possibly promoted by enhanced orientational correlations in the transverse molecular packing (compared to the other BCNs), synthetic efforts are underway to develop variants of these molecules that may be able to extend the local biaxial correlations to the macroscopic scale. Another potentially interesting direction of research might be the measurements of the biaxial susceptibility of the electric field-induced modification of the optical tensor; that would indicate how close the N_u might be to forming N_b in the absence of an electric field [58].

ACKNOWLEDGEMENTS

The authors acknowledge C. Ferrero, D. Hermida Merino and T. Narayanan, ESRF (Grenoble, France), for their support during XRD measurements. E. Scharrer acknowledges NSF DMR-1005923 for financial support. O. D. Lavrentovich's research was supported by grants NSF DMR-1121288 and NSF IIP-1500204.

References

[1] A. Jákli, Liq. Cryst. Rev. **1**, 65 (2013).

[2] C. Tschierske and D. J. Photinos, J. Mat. Chem. **20**, 4263 (2010).

[3] B. R. Acharya, A. Primak, and S. Kumar, Phys. Rev. Lett. **92**, 145506 (2004).

[4] L. A. Madsen, T. J. Dingemans, M. Nakata, and E. T. Samulski, Phys. Rev. Lett. **92**, 145505 (2004).

[5] G. S. Lee, J. S. Cho, J. C. Kim, T.-H. Yoon, and S. T. Shin, J. Appl. Phys. **105**, 094509 (2009).

[6] Y. Jang, V. P. Panov, A. Kocot, J. K. Vij, A. Lehmann, and C. Tschierske, Appl. Phys. Lett. **95**, 183304 (2009).

[7] H. G. Yoon, S.-W. Kang, R. Y. Dong, A. Marini, K. A. Suresh, M. Srinivasarao, and S. Kumar, Phys. Rev. E **81**, 051706 (2010).

[8] M. Nagaraj, K. Merkel, J. K. Vij, and A. Kocot, EPL **91**, 66002 (2010).

[9] B. Senyuk, H. Wonderly, M. Mathews, Q. Li, S. V. Shiyanovskii, and O. D. Lavrentovich, Phys. Rev. E **82**, 041711 (2010).

[10] M. Nagaraj, Y. P. Panarin, U. Manna, J. K. Vij, C. Keith, and C. Tschierske, Appl. Phys. Lett. **96**, 011106 (2010).

[11] M. S. Park, B.-J. Yoon, J. O. Park, V. Prasad, S. Kumar, and M. Srinivasarao, Phys. Rev. Lett. **105**, 027801 (2010).

[12] B. Senyuk, Y.-K. Kim, L. Tortora, S.-T. Shin, S. V. Shiyanovskii, and O. D. Lavrentovich, Mol. Cryst. Liq. Cryst. **540**, 20 (2011).

[13] Y. Jang, V. P. Panov, A. Kocot, A. Lehmann, C. Tschierske, and J. K. Vij, Phys. Rev. Lett. **84**, 060701 (2011).

[14] S. J. Picken, T. J. Dingemans, L. A. Madsen, O. Francescangeli, and E. T. Samulski, Liq. Cryst. **39**, 19 (2012).

[15] Y.-K. Kim, M. Majumdar, B. I. Senyuk, L. Tortora, J. Seltmann, M. Lehmann, A. Jákli, J. T. Gleeson, O. D. Lavrentovich, and S. Sprunt, Soft Matter **8**, 8880 (2012).

[16] Y.-K. Kim, G. Cukrov, J. Xiang, S.-T. Shin, and O. D. Lavrentovich, Soft Matter **11**, 3963 (2015).

[17] O. Francescangeli, S. I. Torgova, L. A. Karamysheva, T. A. Geivandova, A. Strigazzi, V. Stanic, C. Ferrero, and I. Dolbnya, in *Proceedings of the 19th International Liquid Crystal Conference*, *Edinburgh, UK*, *2002*, p. 137.

[18] A. G. Vanakaras and D. J. Photinos, J. Chem. Phys. **128**, 154512 (2008).

[19] O. Francescangeli, V. Stanic, S. I. Torgova, A. Strigazzi, N. Scaramuzza, C. Ferrero, I. P. Dolbnya, T. M. Weiss, R. Berardi, L. Muccioli, S. Orlandi, and C. Zannoni, Adv. Funct. Mater. **19**, 2592 (2009).

[20] O. Francescangeli and E. T. Samulski, Soft Matter **6**, 2413 (2010).

[21] S. H. Hong, R. Verduzco, J. C. Williams, R. J. Twieg, E. DiMasi, R. Pindak, A. Jákli, J. T. Gleeson, and S. Sprunt, Soft Matter **6**, 4819 (2010).

[22] C. Keith, A. Lehmann, U. Baumeister, M. Prehm, and C. Tschierske, Soft Matter **6**, 1704 (2010).

[23] E. T. Samulski, Liq. Cryst. **37**, 669 (2010).

[24] O. Francescangeli, F. Vita, C. Ferrero, T. Dingemans, and E. T. Samulski, Soft Matter **7**, 895 (2011).

[25] C. Zhang, M. Gao, N. Diorio, W. Weissflog, U. Baumeister, S. Sprunt, J. T. Gleeson, and A. Jákli, Phys. Rev. Lett. **109**, 107802 (2012).

[26] T. J. Dingemans, L. A. Madsen, O. Francescangeli, F. Vita, D. J. Photinos, C.-D. Poon, and E. T. Samulski, Liq. Cryst. **40**, 1655 (2013).

[27] O. Francescangeli, F. Vita, and E. T. Samulski, Soft Matter **10**, 7685 (2014).

[28] S. Stojadinovic, A. Adorjan, S. Sprunt, H. Sawade, and A. Jákli, Phys. Rev. E **66**, 060701 (2002).

[29] V. Domenici, C. A. Veracini, and B. Zalar, Soft Matter **1**, 408 (2005).

[30] G. Cinacchi and V. Domenici, Phys. Rev. E **74**, 030701 (2006).

[31] F. Vita, T. Tauscher, F. Speetjens, E. T. Samulski, E. Scharrer, and O. Francescangeli, Chem. Mater. **26**, 4671 (2014).

[32] F. Vita, T. Tauscher, F. Speetjens, C. Ferrero, E. T. Samulski, E. Scharrer, and O. Francescangeli, Mol. Cryst. Liq. Cryst. **611**, 171 (2015).

[33] J. Nguyen, W. Wonderly, T. Tauscher, R. Harkins, F. Vita, G. Portale, O. Francescangeli, E. T. Samulski, and E. Scharrer, Liq. Cryst. **42**, 1754 (2015).

[34] A. Glebowska, F. Vita, O. Francescangeli, T. Dingemans, and E. Samulski, Liq. Cryst. **42**, 829 (2015).

[35] F. Speetjens, J. Lindborg, T. Tauscher, N. LaFemina, J. Nguyen, E. T. Samulski, F. Vita, O. Francescangeli, and E. Scharrer, J. Mater. Chem. **22**, 22558 (2012).

[36] Y.-K. Kim, B. Senyuk, and O. D. Lavrentovich, Nat. Commun. **3**, 1133 (2012).

[37] O. D. Lavrentovich, Y.-K. Kim, and B. I. Senyuk, Proc. of SPIE **OP211**, 84750 (2012).

[38] A. J. Leadbetter, R. M. Richardson, and C. N. Colling, J. Phys. Colloques **36**, C1-37 (1975).

[39] M. Kleman and O. D. Lavrentovich, *Soft matter physics: An introduction* (Springer, New York, 2003).

[40] M. Shribak and R. Oldenbourg, Appl. Optics. **42**, 3009 (2003).

[41] O. D. Lavrentovich, Contemp. Math. **577**, 25 (2011).

[42] Y.-J. Lee, J.-H. Baek, Y. Kim, J. U. Heo, C.-J. Yu, and J.-H. Kim, J. Phys. D: Appl. Phys. **46**, 145305 (2013).

[43] K. Merkel, A. Kocot, J. K. Vij, R. Korlacki, G. H. Mehl, and T. Meyer, Phys. Rev. Lett. **93**, 237801 (2004).

[44] S. Polineni, J. L. Figueirinhas, C. Cruz, D. A. Wilson, and G. H. Mehl, J. Chem. Phys. **138**, 124904 (2013).

[45] Y.-K. Kim, B. Senyuk, S.-T. Shin, A. Kohlmeier, G. H. Mehl, and O. D. Lavrentovich, Soft Matter **10**, 500 (2014).

[46] Y.-K. Kim, R. Breckon, S. Chakraborty, M. Gao, S. N. Sprunt, J. T. Gleeson, R. J. Twieg, A. Jákli, and O. D. Lavrentovich, Liq. Crysts. **41**, 1345 (2014).

[47] V. Borshch, Y.-K. Kim, Y. Xiang, M. Gao, A. Jákli, V. P. Panov, J. K. Vij, C. T. Imrie, M. G. Tamba, G. H. Mehl, and O. D. Lavrentovich, Nat. Commun. **4**, 2635 (2013).

[48] Y.-K. Kim, S. Zhou, G. H. Mehl, S.-T. Shin, A. Jákli, and O. D. Lavrentovich, In Preparation (2016).

[49] R. Oldenbourg, *Polarization microscopy with the LC-polscope* (Cold Spring Harbor Laboratory Press, New York, 2005).

[50] Y.-K. Kim, S. V. Shiyanovskii, and O. D. Lavrentovich, J. Phys.: Condens. Matter **25**, 404202 (2013).

[51] G. E. Volovik and V. P. Mineev, Zh. Eksp. Teor. Fiz. **72**, 2256 (1977) or Sov. Phys. JEPT **45**, 1186 (1977).

[52] M. V. Kurik and O. D. Lavrentovich, Usp. Fiz. Nauk 154, 381 (1988) or Sov. Phys. Usp. **31**, (1988).

[53] S. Ramaswamy, R. Nityananda, V. A. Raghunathan, and J. Prost, Mol. Cryst. Liq. Cryst. **288**, 175 (1996).

[54] P. Poulin and D. A. Weitz, Phys. Rev. E **57**, 626 (1998).

[55] I. I. Smalyukh, O. D. Lavrentovich, A. N. Kuzmin, A. V. Kachynski, and P. N. Prasad, Phys Rev Lett **95**, 157801 (2005).

[56] J. Kotar, M. Vilfan, N. Osterman, D. Babič, M. Čopič, and I. Poberaj, Phys. Lett. A. **96** 207801 (2006).

[57] G. E. Volovik and O. D. Lavrentovich, Zh. Eksp. Teor. Fiz. **85**, 1997 (1983) or Sov. Phys. JETP. **58**, 1159 (1983).

[58] V. Borshch, S. V. Shiyanovskii, B.-X. Li, and O. D. Lavrentovich, Phys. Rev. E **90**, 062504 (2014).